

# Form factor for large quantum graphs: evaluating orbits with time-reversal

Gregory Berkolaiko

Department of Mathematics, University of Strathclyde, Glasgow G1 1XH, UK

PACS numbers: 03.65.N, 05.45.Mt

**Abstract.** It has been shown that for a certain special type of quantum graphs the random-matrix form factor can be recovered to at least third order in the scaled time  $\tau$  using periodic-orbit theory. Two types of contributing pairs of orbits were identified, those which require time-reversal symmetry and those which do not. We present a new technique of dealing with contribution from the former type of orbits.

The technique allows us to derive the third order term of the expansion for general graphs. Although the derivation is rather technical, the advantages of the technique are obvious: it makes the derivation tractable, it identifies explicitly the orbit configurations which give the correct contribution, it is more algorithmical and more system-independent, making possible future applications of the technique to systems other than quantum graphs.

## 1. Introduction

The BGS conjecture [1] asserts that the spectral correlations in quantum systems with chaotic classical analogue fall into several universality classes, depending on the symmetries of the system. In particular, the spectral correlations of systems with time-reversal (TR) symmetry coincide with the relevant expressions obtained in random matrix theory for Orthogonal Ensembles of matrices. This claim was supported by a multitude of numerical examples [2], but for a long time the only theoretical advance for individual systems (i.e. without disorder average) was Berry's diagonal approximation [3]. The recent work of Sieber and Richter [4] and Sieber [5] has renewed the hope that the universality of spectral correlations can be explained within periodic-orbit theory.

One of the more convenient statistics is the Fourier transform of the spectral two-point correlator, the form factor, whose universal expression for Orthogonal Ensembles is given by the formula

$$K_{\text{GOE}}(\tau) = 2\tau - \tau \log(1 + 2\tau) = 2\tau - 2\tau^2 + 2\tau^3 + O(\tau^4), \quad (1)$$

when  $\tau$  is in the range  $0 \leq \tau \leq 1$ . For a quantum chaotic system the form factor can be written in terms of a double sum over periodic orbits (PO) using the Gutzwiller trace-formula [6]. This double sum is the usual starting point for analysis, in which different classes of periodic orbit pairs are identified and their contribution is evaluated to reproduce the small- $\tau$  expansion of the prediction (1).

Berry [3] calculated the form factor, neglecting all correlations between POs other than exact symmetries. Within this “diagonal approximation”, he obtained the leading order term in  $\tau$  expansion. In [4, 5] it was shown, that for uniformly hyperbolic and time-reversal invariant billiards on surfaces with constant negative curvature the second-order contribution  $-2\tau^2$  is related to correlations within pairs of orbits differing in the orientation of one of the two loops resulting from a self-intersection of the orbit. The same result, but without restriction to uniformly hyperbolic dynamics, was derived for a large family of quantum graphs [9]. In particular, some progress has been made in identifying exact requirement on degree of “chaoticity” of the graphs. The further step to third order was performed in [10], where some of the classes of orbits were evaluated for general graphs, but for classes of orbits which explicitly required time-reversal symmetry, the uniform hyperbolicity had to be assumed. At this time it became clear that the method used in [9] would become intractable for the third order in general graphs and deriving the fourth order term would be quite impossible even for systems with uniformly hyperbolic dynamics.

The present manuscript presents a different method of dealing with various classes of orbits. The underlying idea is the repeated application of inclusion-exclusion principle to obtain a decomposition of orbit pairs into sets of which only a relatively small proportion gives nonzero contribution. This technique has several advantages: the derivation becomes tractable for general graphs, the orbit classes giving the universal contributions are identified explicitly, the application of technique is a relatively mechanical process which decreases the chance of missing a contribution and raises hope for a general

derivation of the expansion to all orders. And not the least advantage is that the technique is relatively system-independent in that it does not use any features specific to quantum graphs, operating on rather abstract *diagrams*.

This article is organised as follows: In Section 2 we define our model and explain how the form factor can be expressed as a double sum over periodic orbits. In Section 3 this sum is rewritten in terms of diagrams, representing all orbits with a given number and topology of self-intersections. Diagrams contributing to the first three orders are identified. In Section 4 we explain our method by re-deriving the second order contribution and then proceed to apply it to obtain the third order term.

## 2. Quantum graphs and periodic-orbit theory

We consider graphs with  $N$  vertices connected by a total of  $B$  directed bonds. A bond leading from vertex  $m$  to vertex  $l$  is denoted by  $(m, l)$ . Since we are considering graphs with time-reversal invariance, it is necessary that for any bond  $(m, l)$  there exists also the reversed bond  $(l, m)$ . We do not rule out the possibility of loops, i.e. bonds of the form  $(m, m)$ .

The discrete quantum dynamics on a graph is defined in terms of a  $B \times B$  unitary time-evolution operator  $S^{(B)}$ , which has matrix elements  $S_{m'l',lm}^{(B)}$  describing the transition amplitudes from the directed bond  $(m, l)$  to  $(l', m')$ ‡. The topology of the underlying graph is reflected in the quantum dynamics because the amplitudes are non-zero only if the two bonds are joined at a vertex  $l = l'$ . We choose

$$S_{m'l',lm}^{(B)} = \delta_{l'l} \sigma_{m'm}^{(l)} e^{i\phi_{ml}} \quad (2)$$

with  $\sigma_{m'm}^{(l)}$  denoting the *vertex-scattering matrix* at vertex  $l$ . The phases  $\phi_{ml}$  are random variables distributed uniformly in  $[0, 2\pi]$  and for a fixed  $B$  they define an ensemble of matrices  $S^{(B)}$  which can be used for averaging. It is possible to interpret this ensemble as an infinite energy average for a given quantum graph with rationally independent bond lengths [7]. For a unitary operator like  $S^{(B)}$  the form factor is defined at integer times  $t = 0, 1, \dots$  by

$$K^{(B)}(\tau) = B^{-1} \langle |\text{tr} S^t|^2 \rangle_{\{\phi\}}, \quad (3)$$

where  $\tau$  is the scaled time  $\tau = t/B$ . See [2] for more details on the description of two-point correlations for unitary operators. For finite  $B$ , the form factor (3) should be compared to ensembles of unitary random matrices (COE for systems with time-reversal symmetry). However, we are interested here in the limit of large graphs  $B \rightarrow \infty$ , keeping the scaled time  $\tau$  fixed

$$K(\tau) = \lim_{B \rightarrow \infty} K^{(B)}(\tau), \quad (4)$$

because this is equivalent to the semiclassical limit of chaotic systems [7, 8]. It is in this limit that the form factor is expected to assume the corresponding universal form (1).

‡ We drop the parentheses when a bond is used as an index of a matrix.

Associated with the unitary matrix  $S$  is the doubly stochastic matrix  $M$  with

$$M_{m'l,lm}^{(B)} = |S_{m'l,lm}^{(B)}|^2 = |\sigma_{m'm}^{(l)}|^2. \quad (5)$$

It defines a Markov chain on the graph which represents the classical analogue of our quantum system [7, 8, 12].  $M$  can be considered as the Frobenius-Perron operator of the discrete classical dynamics. Matrix elements of powers of this operator give the classical probability to get from bond  $(m, l)$  to bond  $(k, n)$  in  $t$  steps

$$P_{(m,l) \rightarrow (k,n)}^{(t)} = [M^t]_{nk,lm}. \quad (6)$$

Under very general assumptions it can be shown that the dynamics generated by  $M$  is ergodic and mixing<sup>§</sup>, i. e. for fixed  $B$  and  $t \rightarrow \infty$  all transition probabilities become equal

$$P_{(m,l) \rightarrow (k,n)}^{(t)} \rightarrow B^{-1} \text{ as } t \rightarrow \infty \quad \forall (m, l), (k, n). \quad (7)$$

However, since in (4) the limits  $B \rightarrow \infty$  and  $t \rightarrow \infty$  are connected by fixing  $\tau$ , Eq. (7) is not useful for showing agreement between PO expansion and RMT. We need a stronger condition such as

$$P_{(m,l) \rightarrow (k,n)}^{(\tau B)} \rightarrow B^{-1} \text{ as } B \rightarrow \infty \quad \forall (m, l), (k, n). \quad (8)$$

This was already discussed in [14] in connection with the diagonal approximation. In fact the precise condition may in principle depend on the order to which agreement with RMT is required. However, exponential convergence is sufficient in any case. We will restrict ourselves to graphs which obey this condition rather than derive a more precise condition for the applicability of (8) for the summation of third-order diagrams.

A connection between the quantum form factor (3) and the classical dynamics given by (5) can be established by representing the form factor as a sum over (classical) POs. We expand the matrix powers of  $S$  in (3) and obtain sums over products of matrix elements  $S_{p_2 p_1, p_1 p_t} \cdots S_{p_4 p_3, p_3 p_2} S_{p_3 p_2, p_2 p_1}$ . Obviously each such product can be specified by a sequence of  $t$  vertices. Vertex sequences which are identical up to a cyclic shift give identical contributions and will be combined into the contribution of a periodic orbit  $P = [p_1, \dots, p_t]$ . For most POs there are  $t$  different cyclic shifts. Exceptions to this rule are possible if a PO is a repetition of a shorter orbit, but the fraction of such orbits decreases exponentially in  $t$ . We obtain

$$\text{tr} S^t = t \sum_P A_P e^{i\phi_P} \quad (9)$$

with  $A_P = \prod_{i=1}^t \sigma_{p_{i+1}, p_{i-1}}^{(p_i)}$  and  $\phi_P = \sum_{i=1}^t \phi_{p_{i+1}, p_i}$  (vertex indices are taken modulo  $t$ ). Substituting this into (3) we obtain a double sum over periodic orbits

$$K^{(B)}(\tau) = \frac{t^2}{B} \left\langle \sum_{P,Q} A_P A_Q^* e^{i(\phi_P - \phi_Q)} \right\rangle_{\{\phi\}}. \quad (10)$$

<sup>§</sup> This assumption is plausible if the underlying graph is connected and one excludes special cases like bipartite graphs [13].

We can now perform the average over the phases  $\phi_{ml}$  associated with the directed bonds. Time-reversal symmetry implies that the phases of a pair of bonds related by time-reversal obey  $\phi_{ml} = \phi_{lm}$ . Then the average over the independent variables in (10) results in

$$\left\langle e^{i(\phi_P - \phi_Q)} \right\rangle_{\phi_{lm}} = \delta_{n_{lm}^{(P)} + n_{ml}^{(P)}, n_{lm}^{(Q)} + n_{ml}^{(Q)}}. \quad (11)$$

Thus the averaging amounts to picking out only those pairs of orbits which visit *the same set of bonds, or their time-reverses, the same number of times*. Hence, the form factor for a quantum graph with time-reversal symmetry is

$$K_{\text{TR}}^{(B)}(\tau) = \frac{t^2}{B} \sum_{P,Q} A_P A_Q^* \left[ \prod_{l \geq m} \delta_{n_{lm}^{(P)} + n_{ml}^{(P)}, n_{lm}^{(Q)} + n_{ml}^{(Q)}} \right]. \quad (12)$$

### 3. The expansion in self-intersections of the periodic orbits

#### 3.1. From orbits to diagrams

The calculation of the form factor is now reduced to a combinatorial problem: The sum over the pairs  $P, Q$  in (12) must be organized such that the condition

$$n_{lm}^{(P)} + n_{ml}^{(P)} = n_{lm}^{(Q)} + n_{ml}^{(Q)} \quad (13)$$

is satisfied. This can be done by composing  $P$  and  $Q$  from the same segments, or *arcs*, which appear in  $P$  and  $Q$  in different order and/or orientation. This is possible if the orbit  $P$  contains self-intersections, i.e. vertices which are traversed more than once. See Fig. 1 for examples. In general an orbit  $P$  has many self-intersections and many partner orbits  $Q$  satisfying Eqs. (13) and the summation over all possible  $Q$  for a fixed  $P$  is too complicated. Instead we fix a transformation: a permutation of arcs followed by the time reversal of selected arcs. Then we sum over all possible pairs of orbits  $P, Q$  related by this transformation. The clearest way to represent all possible transformations is graphical, hence we refer to them as diagrams. The sum over all diagrams finally gives the form factor.

The main problem with this approach is to ensure that each orbit pair  $P, Q$  is counted once and only once. This is difficult because for a given pair  $P, Q$  the identification of the arcs and their permutation, transforming  $P$  into  $Q$ , is not necessarily unique. As a simple example consider the diagrams on Fig. 1. Part (a) gives a schematic representation of the pair  $P, Q$  where  $Q$  is obtained from  $P$  by reversal of arc 2. Such orbits were considered in [9] and were shown to give the contribution  $-2\tau^2$ . One of the difficult points of the derivation was correct counting of the orbits which do not merely cross but follow itself for at least one bond: an example of such orbit is given in part (b). For this orbit, there are two possibilities to identify arc 1: either as  $\rightarrow a \rightarrow b \rightarrow$  or as  $\rightarrow c \rightarrow a \rightarrow b \rightarrow c \rightarrow$ , thus taking either  $c$  or  $d$  as the intersection point.

To avoid this double-counting, [9] imposed *restriction* on arc 1. Denoting the first vertex of the arc as  $s_1$  and the last one as  $f_1$ , it was demanded that  $s_1 \neq f_1$ . This

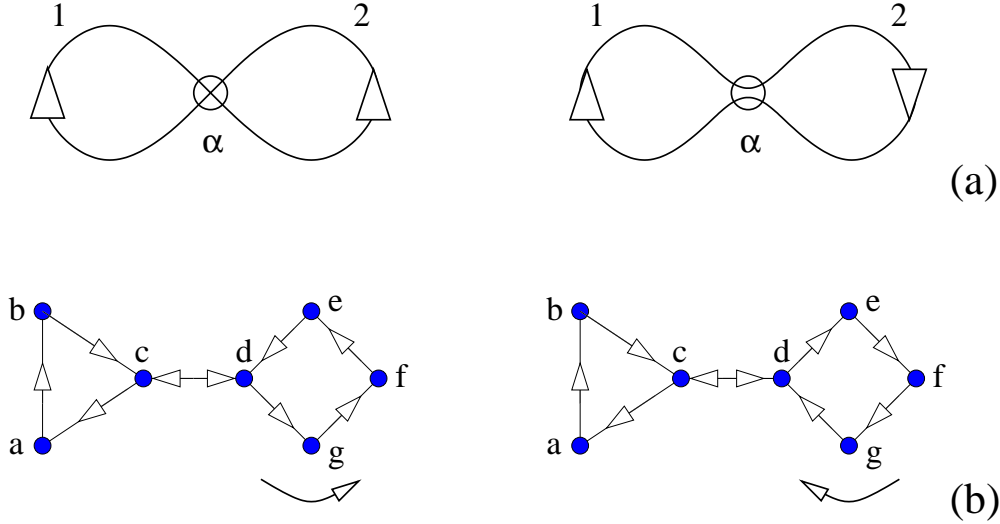


**Figure 1.** A schematic representation of an orbit with a self-intersection at a vertex  $\alpha$  and its partner orbit (a). There are orbits, however, for which the position of the intersection point  $\alpha$  is ambiguous. The pair of orbits shown on (b) can be fitted into the pattern (a) with either  $c$  or  $d$  playing the role of the intersection vertex.

insured the unique choice of the arcs and the intersection point. In the example above, the valid choice is  $\rightarrow a \rightarrow b \rightarrow$ .

Unfortunately, even with this restriction, there were orbits that should not be counted: those *exceptions* had self-retracing arc 2. The self-retracing arc did not change under time-reversal and as a result, the orbit  $Q$  was identical to the orbit  $P$ , forming a pair which was already counted in the diagonal approximation. The contribution of such orbits had to be subtracted explicitly.

In this paper we present a different counting technique, which is easily extendable to more complicated diagrams, avoids the introduction of exceptions and explicitly identifies the orbits which give the generic contribution. We will first illustrate our approach by rederiving the  $-2\tau^2$  contribution and then proceed to calculate the third order correction. But before we can do it, we need to introduce the notation and discuss some preliminary matters.

### 3.2. Notation

If we consider  $P$  as a single arc with no intersections,  $Q = P$  and  $Q = \overline{P}$  are the only options. The corresponding diagram have a simple circular shape (the first diagram of Fig. 2). Summation over these orbit pairs is nothing other than the diagonal approximation. It produces  $K_1 = 2\tau$ . In [9] orbit  $P$  was treated as two arcs, 1 and 2, joined at a single intersection  $\alpha$ , corresponding to an 8-shaped diagram, Fig. 2. The contributions of such orbits were found to give rise to the second-order term in (1)  $K_2 = -2\tau^2$ . In this paper we calculate the  $\tau^3$ -contribution by assuming that  $P$  contains three or four arcs connected at intersections.

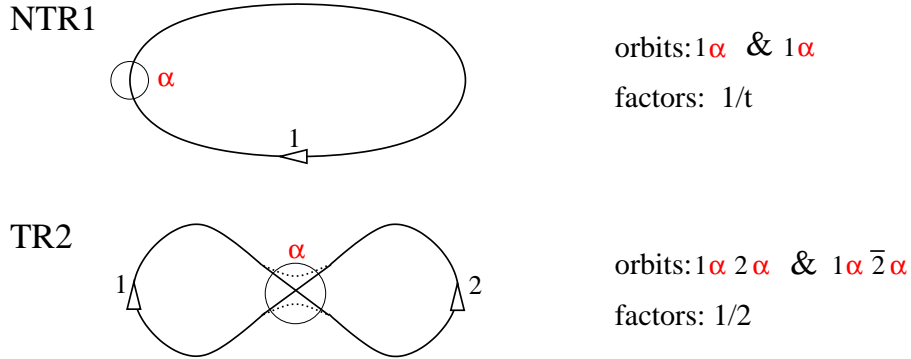


**Figure 2.** Topology of orbits contributing to form factor at first and second orders. Evaluating the orbits from NTR1 we recover the diagonal approximation to the form factor.

We denote arcs by numbers  $1, 2, \dots$  and the intersection points by Greek letters  $\alpha, \beta, \dots$ . An arc can be identified by a sequence of vertices, which does not include the intersection vertices, or, alternatively, by a sequence of bonds, which includes the bonds from and to the intersection points. The length of the  $i$ th arc is denoted by  $t_i$  and is defined as the number of bonds in the arc (which is one more than the number of vertices in the arc). The sum of the lengths of all arcs gives  $t$ , the length of the orbit. The length of an arc is at least one. Given an arc  $i$  leading from  $\alpha$  to  $\beta$  we denote the first vertex following  $\alpha$  by  $s_i$  and the last vertex before  $\beta$  by  $f_i$ . In the degenerate case when the arc going from  $\alpha$  to  $\beta$  is the single bond  $(\alpha, \beta)$  and does not contain any vertices ( $t_i = 1$ ) our definition implies  $s_i = \beta$  and  $f_i = \alpha$ . The time reversal of an arc is indicated by the bar over the arc's number, e.g.  $\bar{1}$ .

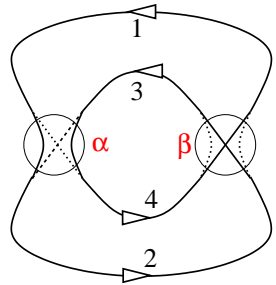
The diagrams contributing at the third order are shown on Figs. 3. For a discussion why only these particular diagrams contribute at third order in  $\tau$  we refer the reader to [10]. In any diagram, the arcs forming an orbit  $P$  and its partner  $Q$  are identical, but the way they are connected at the intersections differs. The orbit  $P$  is given by the connections drawn as continuous lines, while its partner orbit  $Q$  is given by connections drawn as dotted lines. The orbits  $P$  and  $Q$  are also written as a symbolic code to the right of each diagram: a path that goes from the beginning of arc 1 to vertex  $\alpha$  then on arc 2 to vertex  $\beta$  and so on is denoted as  $1\alpha 2\beta \dots$ . The diagrams divide into two classes, NTR and TR. In the NTR-diagrams all the arcs of  $Q$  have the same orientation as the corresponding arcs in  $P$ , while in the TR-diagrams some of the arcs of  $Q$  are time-reversed. For a system with no time-reversal symmetry, only the NTR-diagrams are possible. In our case, diagrams in both classes contribute and  $\tau^3$ -contributions to the form factor is a sum of five terms

$$K_3 = 2(K_{\text{NTR3a}} + K_{\text{NTR3b}} + K_{\text{TR3a}} + K_{\text{TR3b}} + K_{\text{TR3c}}). \quad (14)$$

The factor of two is due to the fact that for every diagram in Fig. 3 there is another one with  $Q$  replaced by its complete time-reversal,  $\bar{Q}$ , which gives an identical contribution.

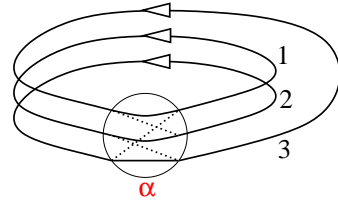
The NTR-diagrams were treated in the general case in [10] and in this manuscript

NTR3a



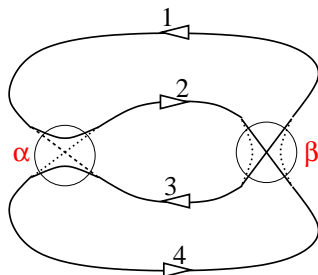
orbits:  $1\alpha 2\beta 3\alpha 4\beta$  &  $1\alpha 4\beta 3\alpha 2\beta$   
 factors: 1/4

NTR3b



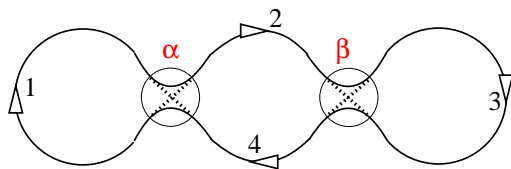
orbits:  $1\alpha 2\alpha 3\alpha$  &  $1\alpha 3\alpha 2\alpha$   
 factors: 1/3

TR3a



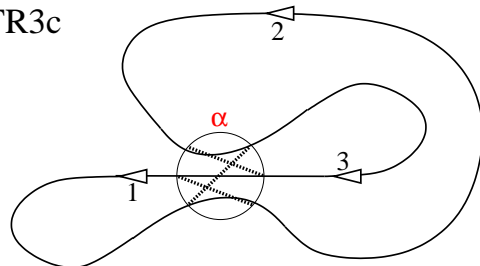
orbits:  $1\alpha 2\beta 3\alpha 4\beta$  &  $1\alpha 4\beta \bar{2}\alpha \bar{3}\beta$   
 factors: 1/2

TR3b



orbits:  $1\alpha 2\beta 3\beta 4\alpha$  &  $1\alpha \bar{4}\beta 3\beta \bar{2}\alpha$   
 factors: 1/2

TR3c



orbits:  $1\alpha 2\alpha 3\alpha$  &  $1\alpha 3\alpha \bar{2}\alpha$   
 factors: 1

**Figure 3.** Topology of NTR3a, NTR3b, TR3a, TR3b and TR3c. In each case a pair of orbits is shown, one follows the solid line throughout, the second follows the solid line except at the intersections (denoted by circles) where it follows the dotted line. Each circle represents a single vertex where a self-intersection of the orbit occurs. Next to each topology we give the symbolic code for the pair and the corresponding weight factor (Section 3.3).

we derive the contribution of TR-diagrams using a slightly different method.

### 3.3. Avoiding double-counting

There are degeneracies in the diagrams which can be accounted for by simple prefactors multiplying the contributions like the factor of two in (14). These factors were derived in [10] and are listed in Fig. 3 next to the diagrams.

Another potential source for double-counting of orbits are *tangential* intersections, already mentioned in Section 3.1. By a tangential intersection we mean the situation where an orbit does not merely cross itself but follows itself for at least one bond. Double-counting can be avoided using a method outlined in [9] and followed in [10]: the intersection point is uniquely defined by ruling that if there is an ambiguity then the intersection is as far to one side as possible. As an example we refer to the ambiguous intersections in Fig. 1(b) and insist the intersection is as far to the left as possible. That is, we demand that the vertices  $a$  and  $b$  are distinct.

Contrary to what was done in [10], we will not fix the restrictions for the TR diagrams. The restrictions we choose will depend on the lengths of individual arcs, as will be shown in Section 4.

It should be emphasised that the orbits with tangential self-intersections are responsible for non-zero contributions to the form factor and their correct treatment is absolutely crucial to the derivation.

### 3.4. Orbit amplitudes

Before we can attempt the summation over all orbit pairs  $P, Q$  within a given diagram, we need to understand the structure of the product  $A_P A_Q^*$  appearing in (12). We consider the diagram NTR3b as an example. Let arc 1 be of length  $t_1$ , consisting of the vertices  $[s_1, x_2, x_3, \dots, x_{t_1-2}, f_1]$ . Then both  $A_P$  and  $A_Q$ , will contain factors  $\sigma_{x_2, \alpha}^{(s_1)}, \sigma_{x_3, x_1}^{(x_2)}, \sigma_{x_4, x_2}^{(x_3)} \dots \sigma_{\alpha, x_{t_1-3}}^{(x_{t_1-2})}$ . Thus when we evaluate the product  $A_P A_Q^*$ , the contribution of the arc 1 will come in the form

$$|\sigma_{x_2, \alpha}^{(s_1)} \sigma_{x_3, x_1}^{(x_2)} \sigma_{x_4, x_2}^{(x_3)} \dots \sigma_{\alpha, x_{t_1-3}}^{(x_{t_1-2})}|^2 = P_{(\alpha, x_1) \rightarrow (x_1, x_2) \rightarrow (x_2, x_3) \rightarrow \dots \rightarrow (f_1, \alpha)} \equiv P_1, \quad (15)$$

which is the *classical* probability of following arc 1 from bond  $(\alpha, s_1)$  to bond  $(f_1, \alpha)$ ||. An analogous consideration for the arcs 2 and 3 leads to the probabilities  $P_2$  and  $P_3$ . The factors not yet accounted for in  $P_1, P_2, P_3$  are the transition amplitudes picked up at the intersection vertex  $\alpha$ :

$$A_P A_Q^* = P_1 \times P_2 \times P_3 \times \sigma_{f_3, s_1}^{(\alpha)} \sigma_{f_1, s_2}^{(\alpha)} \sigma_{f_2, s_3}^{(\alpha)} \times \left( \sigma_{f_2, s_1}^{(\alpha)} \sigma_{f_1, s_3}^{(\alpha)} \sigma_{f_3, s_2}^{(\alpha)} \right)^*. \quad (16)$$

To evaluate the contribution of a given diagram a product like (16) must be summed over all free parameters, namely all intersection points and all possible arcs connecting these points. The latter summation includes a sum over the lengths  $t_i$  of these arcs with the restriction that the total length of the orbit is  $t$ .

||  $P_1 = 1$  if arc 1 contains no vertices, i. e. if  $t_1 = 1$ .

The summation over all the intermediate vertices  $x_2, x_3, \dots, x_{t_1-2}$  along arc 1 can be performed immediately, because it is unaffected by the restrictions discussed in the previous subsection: This summation adds the classical probabilities of all possible paths leading from bond  $(\alpha, s_1)$  to bond  $(f_1, \alpha)$  in  $t_1 - 1$  steps and results consequently in the classical transition probability  $P_{(\alpha, s_1) \rightarrow (f_1, \alpha)}^{(t_1-1)}$  given by (6). Analogous summations over the other arcs produce  $P_{(\alpha, s_2) \rightarrow (f_2, \alpha)}^{(t_2-1)}$  and  $P_{(\alpha, s_3) \rightarrow (f_3, \alpha)}^{(t_3-1)}$ . The above approach extends trivially to the TR diagrams when we note that time-reversal symmetry implies that the matrices  $\sigma^{(v)}$  are symmetric.

The remaining summation is over the lengths  $t_i$  of all arcs, the first and the last vertex  $s_i$  and  $f_i$  of all arcs  $i$  with  $t_i > 1$  and the intersection points like  $\alpha$ . For general graphs this sum is still too complicated for explicit calculations, mainly because transition probabilities like  $P_{(\alpha, s_1) \rightarrow (f_1, \alpha)}^{(t_1-1)}$  can be complicated expressions which are not explicitly known. For sufficiently long arcs, however, these transition probabilities can be replaced by  $B^{-1}$  according to (8). Then the sum over vertices decouples into a product of sums associated with each self-intersection vertex  $\alpha$  which can finally be evaluated using the unitarity of the vertex-scattering matrices  $\sigma_\alpha$ . This is the strategy we shall follow in the next two sections, where explicit summation of the NTR3 and TR3 diagrams is performed.

## 4. Summation of TR diagrams

### 4.1. TR2

As was mentioned earlier, we develop a slightly different technique to deal with the TR orbits. We will illustrate it by first considering the TR2 contribution. In [9] we dealt with the intersection point ambiguity by imposing a restriction  $s_2 \neq f_2$ . The summation then would take the form

$$K_{\text{TR2}}(\tau) = \frac{1}{2} \frac{t^2}{B} \sum_{\{t_i\}} \delta \left[ t - \sum_{i=1}^2 t_i \right] \times \sum_{\alpha} \sum_{\{s_i, f_i\}} \Sigma_{\text{TR2}} \times P_{\text{TR2}} \times \Delta_{\text{TR2}} , \quad (17)$$

where

$$\Sigma_{\text{TR2}} = \sigma_{f_2 s_1}^\alpha \sigma_{f_1 s_2}^\alpha \sigma_{s_2 s_1}^{\alpha*} \sigma_{f_1 f_1}^{\alpha*} \quad (18)$$

$$P_{\text{TR2}} = P_{(\alpha, s_1) \rightarrow (f_1, \alpha)}^{t_1-1} P_{(\alpha, s_2) \rightarrow (f_2, \alpha)}^{t_2-1} \quad (19)$$

$$\Delta_{\text{TR2}} = (1 - \delta_{s_2 f_2}) . \quad (20)$$

Since at least one of the arcs must be long, we can approximate the corresponding  $P_{(\alpha, s_i) \rightarrow (f_i, \alpha)}^{t_i-1}$  by its ergodic limit  $1/B$ . If arc 1 is long, we can perform the summation over  $s_1$  (and  $f_1$ )

$$(1 - \delta_{s_2 f_2}) \sum_{s_1} \sigma_{f_2 s_1}^\alpha \sigma_{s_2 s_1}^{\alpha*} = (1 - \delta_{s_2 f_2}) \delta_{s_2 f_2} \equiv 0 \quad (21)$$

to show that the contribution of such orbits is zero. The simplicity ends here, however, as the case when arc 2 is long is not nearly as easy. We can still sum over  $s_2$  or  $f_2$ ,

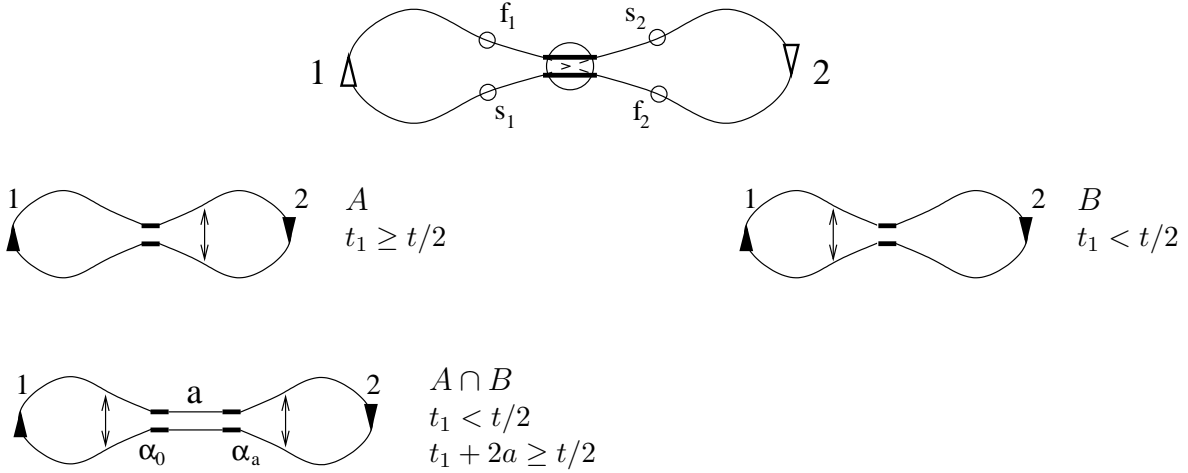


**Figure 4.** The TR2 diagram and its partition into two sets of orbits. The total contribution of the orbits in each set is easily shown to be zero. The result comes from the orbits lying in the intersection of the two sets,  $A \cap B$ .

but the restriction, which helped us in the first part, now stands in the way (see [9] for details).

The idea that we are going to use is as follows: we can change the restrictions depending on the arc lengths. In TR2 case, if arc 1 is long, we stick with the restriction  $s_2 \neq f_2$ , and if arc 2 is long, we switch to the restriction  $s_1 \neq f_1$ . In the first case the result of the summation is 0, as was shown above. In the second case we approximate  $P_{(\alpha, s_2) \rightarrow (f_2, \alpha)}^{t_2-1}$  by  $1/B$  and perform the summation over  $s_2$  to obtain

$$(1 - \delta_{s_1 f_1}) \sum_{s_1} \sigma_{f_1 s_2}^\alpha \sigma_{s_2 s_1}^{\alpha*} = (1 - \delta_{s_1 f_1}) \delta_{s_1 f_1} \equiv 0. \quad (22)$$

This is not what we should be getting: the overall result should be  $-2\tau^2$ , not 0. The reason for getting 0 is that there are orbits which were counted in both sums. To explain this, we need to define more carefully what is meant by “arc  $i$  is long”.

We split the set of all TR2 orbit pairs into two sets. The set  $A$  will contain orbits satisfying  $t_1 \geq t/2$  and  $s_2 \neq f_2$ . The set  $B$  will contain orbits satisfying  $t_1 < t/2$  and  $s_1 \neq f_1$ . The sum of contributions coming from each set is zero, as was shown in previous paragraph. However, these sets are not disjoint. Fig. 4 illustrates both sets, denoted by  $A$  and  $B$ , and the shape of the orbits belonging to their intersection  $A \cap B$ . These are orbits with a tangential intersection which is roughly in the middle of them:  $t_1 < t/2$  but  $t_1 + 2a \geq t/2$ , where  $a$  is the length of the intersection and  $t_1$  is now counted from the end of the tangential intersection (i.e. from vertex  $\alpha_0$ ). We need to subtract the contribution of such orbits to recover the full term  $K_{\text{TR2}}(\tau)$ .

To calculate the contribution of the orbits in  $A \cap B$ , we notice (see Appendix A) that we get the same contribution if we modify the set  $A \cap B$  by setting  $a = 1$  and dropping the constraints. Thus we can write for this contribution (for some fixed  $t_1$  and

$t_2)$

$$\frac{t^2}{2B} \sum_{\alpha_0, \alpha_1} P_{(\alpha_1, \alpha_0) \rightarrow (\alpha_0, \alpha_1)}^{t_1+1} P_{(\alpha_0, \alpha_1) \rightarrow (\alpha_1, \alpha_0)}^{t_2+1} = \frac{t^2}{2B^3} \sum_{\alpha_0, \alpha_1} 1 = \frac{t^2}{2B^2} \rightarrow \frac{\tau^2}{2}, \quad (23)$$

where the last sum is taken over all *connected* pairs of vertices  $\alpha_0$  and  $\alpha_1$ . This result is obtained for a fixed choice of  $t_i$ . But  $t_2 = t - t_1$  and with  $a = 1$ ,  $t_1$  must satisfy  $t_1 < t/2$  and  $t_1 + 2 \geq t/2$ . Thus there are only two possible values that  $t_1$  can take,  $t/2 - 1$  and  $t/2 - 2$ . To get the final result for  $K_{\text{TR2}}(\tau)$ , we need to multiply  $\tau^2/2$  by 2 (for the number of possible values of  $t_1$ ), add minus in front of it (because these orbits were double-counted when we calculated the contributions of the sets  $A$  and  $B$ ), and multiply by two yet again (time-reversal symmetry). Hence obtaining the sought-after result  $K_{\text{TR2}}(\tau) = -2\tau^2$ . It is important to note that in the above derivation we could have used any  $O(t)$  value instead of  $t/2$ .

Now our strategy of dealing with the diagrams of higher order is clear. We will strive to partition the orbits belonging to each diagram into several sets, such that the contribution of each set is easily seen to be zero. The intersections of these sets will provide the true contributions to the form factor. Hopefully, the arcs of the orbits in the intersections will be long and thus the ergodic approximation can be employed to simplify the calculations.

#### 4.2. Partition of TR3a

Before we start making partitions of the diagrams, we stress that there is no unique “right” way to partition. The partition that we are presenting here is only one of those that we considered. All partitions produce the same results, as they should, but the present one seemed to be the least difficult.

The suggested partition for the diagram TR3a is given by Fig. 5 (upper part). Each of the 4 subsets of TR3a is equipped with its own set of constraints, which are shown by the arrows. For example, the set  $A$  has constraints  $f_1 \neq f_3$  and  $s_3 \neq f_4$ . The constraints are chosen in such a way that the contributions of each set evaluate to zero: for example, the arc 1 is long in the set  $A$ , so we can approximate the contribution of the arc by its ergodic limit and subsequently sum over  $s_1$  to obtain zero. The constraints also take into account the symmetry of the diagram: under the permutation of arcs  $1 \leftrightarrow 3$  and  $2 \leftrightarrow 4$ , the set  $A$  is interchanged with  $C$  and  $B$  is interchanged with  $D$ . Also, it is immediately obvious that the sets  $A$  and  $B$  are disjoint; so are the sets  $C$  and  $D$ . Therefore we do not have to worry about 3-way intersections of the partition sets.

Three of the 2-way intersections are straightforward to evaluate, see Fig. 5. The intersection  $A \cap D$  has  $t_1 + t_2 \approx t/2$ , therefore  $t_3 + t_4 \approx t/2$  but  $t_3 + b < t/4$ , therefore the arc 4 is long and we can sum over  $s_4$  obtaining zero. The intersections  $B \cap C$  and  $B \cap D$  can be considered together, as  $B \cap (C \cup D)$ . For this set we again have  $t_1 + t_2 \approx t/2$  and  $t_1$  is small, thus enabling us to sum over  $s_2$ .

The last intersection,  $A \cap C \equiv E$  is the hardest, see Fig. 6. Arcs 2 and 4 are potentially short and summation over any other arc is obstructed by the constraints.

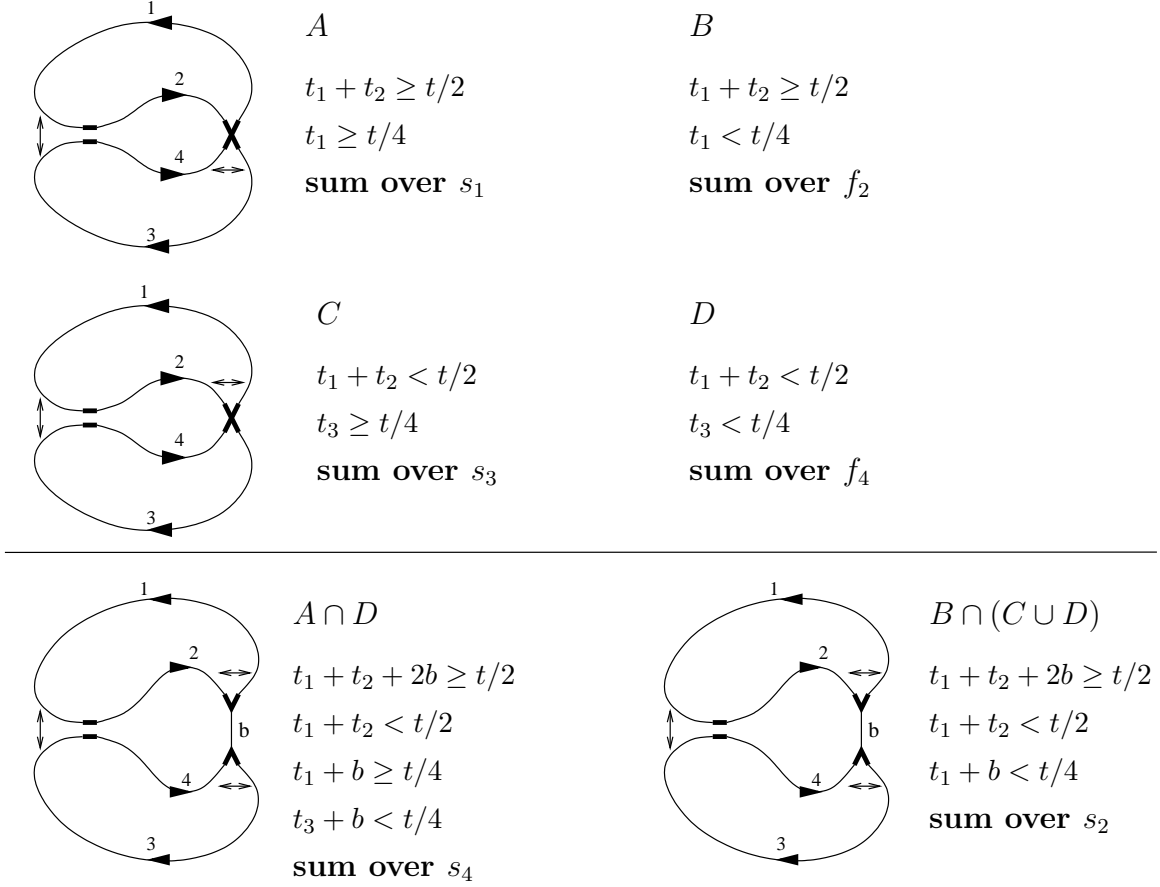


**Figure 5.** The TR3a diagram and its partition into four sets of orbits. The orbits of the sets  $A$  and  $B$  have identical structure but different lengths. The same applies to the sets  $C$  and  $D$ . A consequence of this is that  $A \cap B = C \cap D = \emptyset$  which implies that all 3-way intersections are empty. The contribution of the orbits in each set can be easily shown to be zero. Also drawn on the Figure are three of the four 2-way intersections among the partition sets of the TR3a diagram. The contribution of each is zero.

To overcome this, we change the constraint  $f_1 \neq f_3$  to  $s_2 \neq s_4$ , thus producing the set  $E_1$ . There are certain orbits, however, that belong to  $E$  and do not belong to  $E_1$  and vice versa. These are put into the sets  $E_2$  and  $E_3$ , correspondingly. The orbits from the set  $E_1$  can be easily shown to produce zero contribution. The contribution of the sets  $E_2$  and  $E_3$  are not zero and will be evaluated separately.

#### 4.3. Partition of TR3b

The diagram TR3b is split into three sets, Fig. 7. Here  $r$  is a large number, of order  $t/4$ . The reason we do not just put it equal to  $t/4$  is to highlight the interaction of the diagram TR3b with TR3c.

To show that contribution of the sets  $A$  and  $B$  is zero, simply sum over  $s_1$  and  $s_3$ , correspondingly. In set  $C$ , at least one of the arcs 2 and 4 is long, thus enabling us to

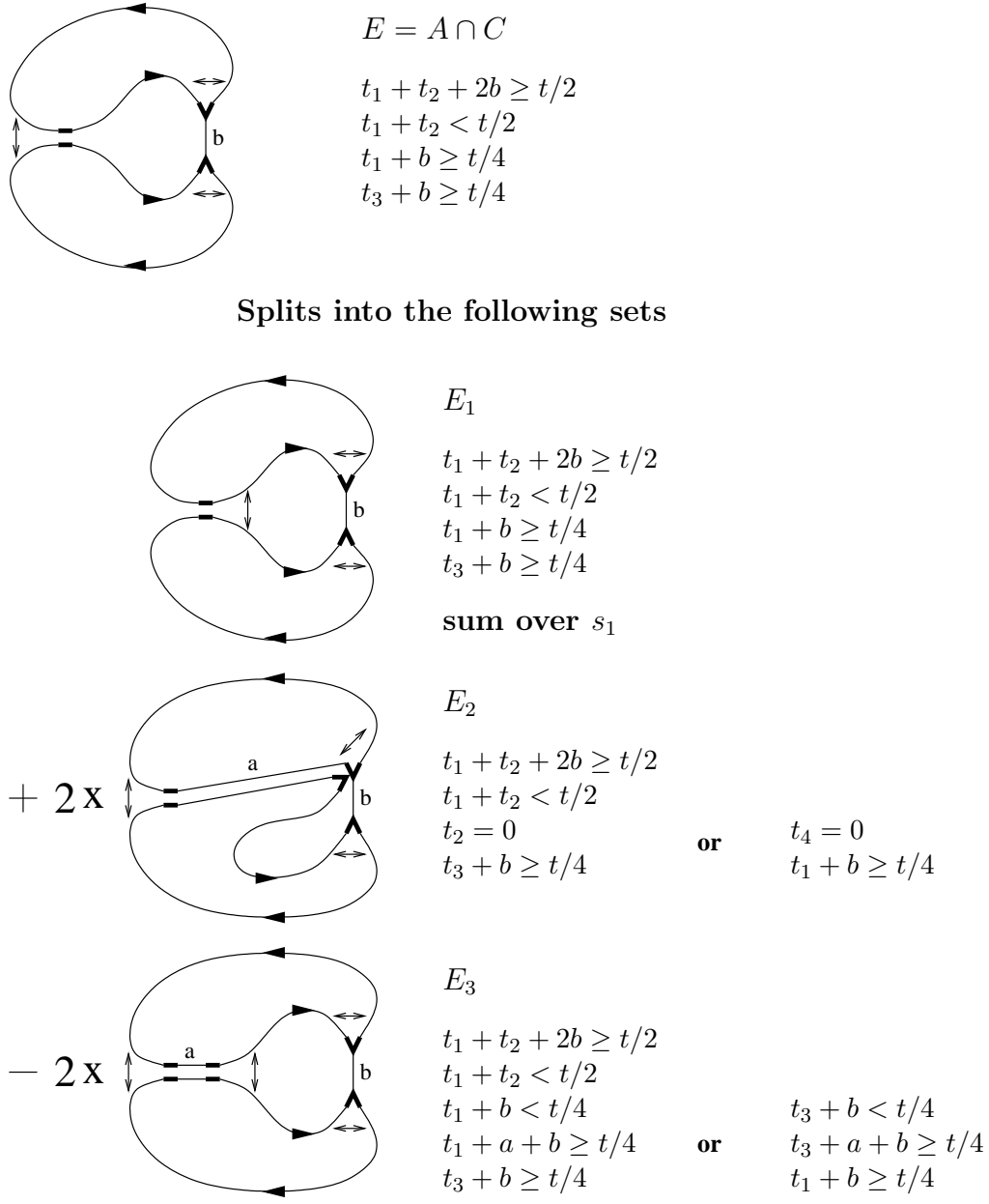


**Figure 6.** The last of the 2-way intersections among the partition sets of the TR3a diagram. To evaluate it we represent it as the set  $E_1$  plus the orbits in the set  $E_2$  minus the orbits of the set  $E_3$ . The contribution of the set  $E_1$  is zero.

sum over  $s_2$  or  $s_4$ . It is easy to see that the sets  $A$  and  $B$  are disjoint.

The intersection  $A \cap C$  is also shown on Fig. 7. One of the arcs 2 and 4 must be long. To be able to sum, we need to drop the restriction  $f_2 \neq s_4$ , producing the set  $F_1$ . By summing either over  $f_2$  or  $s_4$  (depending on which arc is long), we show that the contribution of  $F_1$  is zero. However, the set  $F_1$  is larger than  $A \cap C$ : it includes the orbits sketched in the sets  $F_2$ , those can be obtained if, say, arc 4 is one bond long and  $f_2 = s_4$ . The set  $F_2$  provides a non-zero contribution and will be evaluated separately.

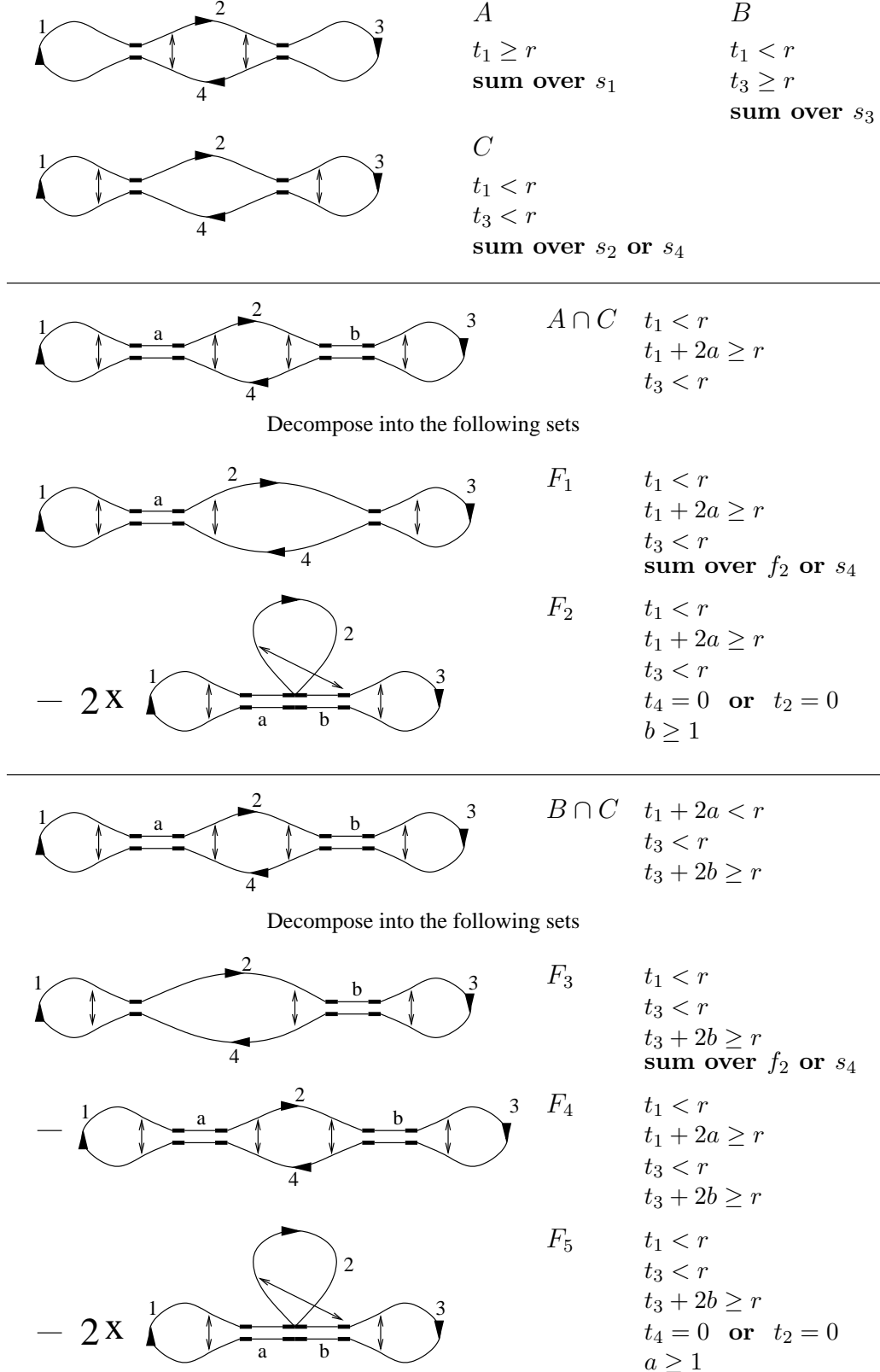


**Figure 7.** The TR3b diagram and its partition into three sets of orbits. The contribution of the orbits in each set can be easily shown to be zero. Below the line we sketch the intersection of the sets  $A$  and  $C$ , repartitioned as  $F_1$  minus  $F_2$  and the sets  $B$  and  $C$ , repartitioned as  $F_3$  minus  $F_4$  and  $F_5$ .

TR3c	TR3a	Lengths			
$f_2 = f_1$	$s_2 = s_4$ ( $t'_2 = 1$ )	$t'_1 = t_1 - 1$	$t'_2 = 1$	$t'_3 = t_2 - 1$	$t'_4 = t_3 + 1$
$s_2 = f_3$	$s_1 = f_2$ ( $t'_2 = 1$ )	$t'_1 = t_1 + 1$	$t'_2 = 1$	$t'_3 = t_2 - 1$	$t'_4 = t_3 - 1$
$s_1 = f_2$	$s_3 = f_4$ ( $t'_3 = 1$ )	$t'_1 = t_1 - 1$	$t'_2 = t_2 - 1$	$t'_3 = 1$	$t'_4 = t_3 + 1$
$s_2 = s_3$	$f_1 = f_3$ ( $t'_3 = 1$ )	$t'_1 = t_1 + 1$	$t'_2 = t_2 - 1$	$t'_3 = 1$	$t'_4 = t_3 - 1$
$s_1 = f_2$ R	$s_1 = f_2$ ( $t'_1 = 1$ )	$t'_1 = 1$	$t'_2 = t_3 + 1$	$t'_3 = t_1 - 1$	$t'_4 = t_2 - 1$
$s_2 = s_3$ R	$f_1 = f_3$ ( $t'_1 = 1$ )	$t'_1 = 1$	$t'_2 = t_3 - 1$	$t'_3 = t_1 + 1$	$t'_4 = t_2 - 1$
$s_2 = f_3$ R	$s_3 = f_4$ ( $t'_4 = 1$ )	$t'_1 = t_2 - 1$	$t'_2 = t_3 - 1$	$t'_3 = t_1 + 1$	$t'_4 = 1$
$f_1 = f_2$ R	$s_2 = s_4$ ( $t'_4 = 1$ )	$t'_1 = t_2 - 1$	$t'_2 = t_3 + 1$	$t'_3 = t_1 - 1$	$t'_4 = 1$
TR3c	TR3b	Lengths			
$s_1 = f_1$	$s_2 = f_4$	$t'_1 = t_1 - 2$	$t'_2 = t_2 + 1$	$t'_3 = t_3$	$t'_4 = 1$
	$s_4 = f_2$	$t'_1 = t_3$	$t'_2 = 1$	$t'_3 = t_1 - 2$	$t'_4 = t_2 + 1$
$s_3 = f_3$	$s_4 = f_2$	$t'_1 = t_1$	$t'_2 = t_2 + 1$	$t'_3 = t_3 - 2$	$t'_4 = 1$
	$s_2 = f_4$	$t'_1 = t_3 - 2$	$t'_2 = 1$	$t'_3 = t_1$	$t'_4 = t_2 + 1$

**Table 1.** Summary of conversions between degenerate orbits of TR3c and two other diagrams. Here  $t_i$  denotes the length of  $i$ th arc in the diagram TR3c and  $t'_i$  denotes the same but for the diagrams TR3a and TR3b; an ‘R’ denotes that the diagram is reversed. For example, the TR3c orbit with  $f_1 = f_2$  can be also considered as a TR3a orbit with  $s_2 = s_4$  and lengths of the arcs given by  $t'_1 = t_1 - 1$ ,  $t'_2 = 1$ ,  $t'_3 = t_2 - 1$  and  $t'_4 = t_3 + 1$

In a similar fashion we treat the intersection  $B \cap C$ , which has to be split into the sets  $F_3$ ,  $F_4$  and  $F_5$ . The contribution of the set  $F_3$  is zero and the sets  $F_4$  and  $F_5$  will be treated separately.

#### 4.4. Partition of TR3c

The diagram TR3c is very special as the orbits belonging to it can also be obtained as orbits from TR3a or/and TR3b when one of the  $t_i$  is equal to zero. Our job is to synchronise the partition of TR3c with the partitions we chose for TR3a and TR3b. The relations between TR3c and other diagrams are summarised in Table 1.

An immediate consequence is that all TR3c orbits with  $f_1 = f_2$  were already counted in TR3a: no set in TR3a has the restriction  $s_2 \neq s_4$ . Also *some* of the orbits from TR3c with  $s_2 = f_3$  are counted in the sets  $A$  and  $C$  of TR3a. To understand precisely which orbits were counted, we notice that a TR3c orbit with  $s_2 = f_3$  corresponds to a TR3a orbit with  $s_1 = f_2$  and  $t'_2 = 1$ . Such orbit can only belong to the set  $A$ , requiring  $t'_1 + t'_2 \geq t/2$  and  $t'_1 \geq t/4$ , which is equivalent to  $t_1 \geq t/2 - 2$  (see the “Lengths” column of the table). Same applies to the reversed orbits from TR3c with  $s_2 = f_3$  which were counted in TR3a set  $C$ . Thus orbits from TR3c with  $t_1 \geq t/2 - 2$  must have the restriction  $s_2 \neq f_3$  (set  $A$  of Fig. 8). We also note that orbits from TR3c with  $s_1 = f_2$  and  $t_3 \geq t/2 - 2$  were already counted in TR3a sets  $B$  and  $D$ , warranting the use of corresponding restriction for the set  $B$  of Fig. 8.

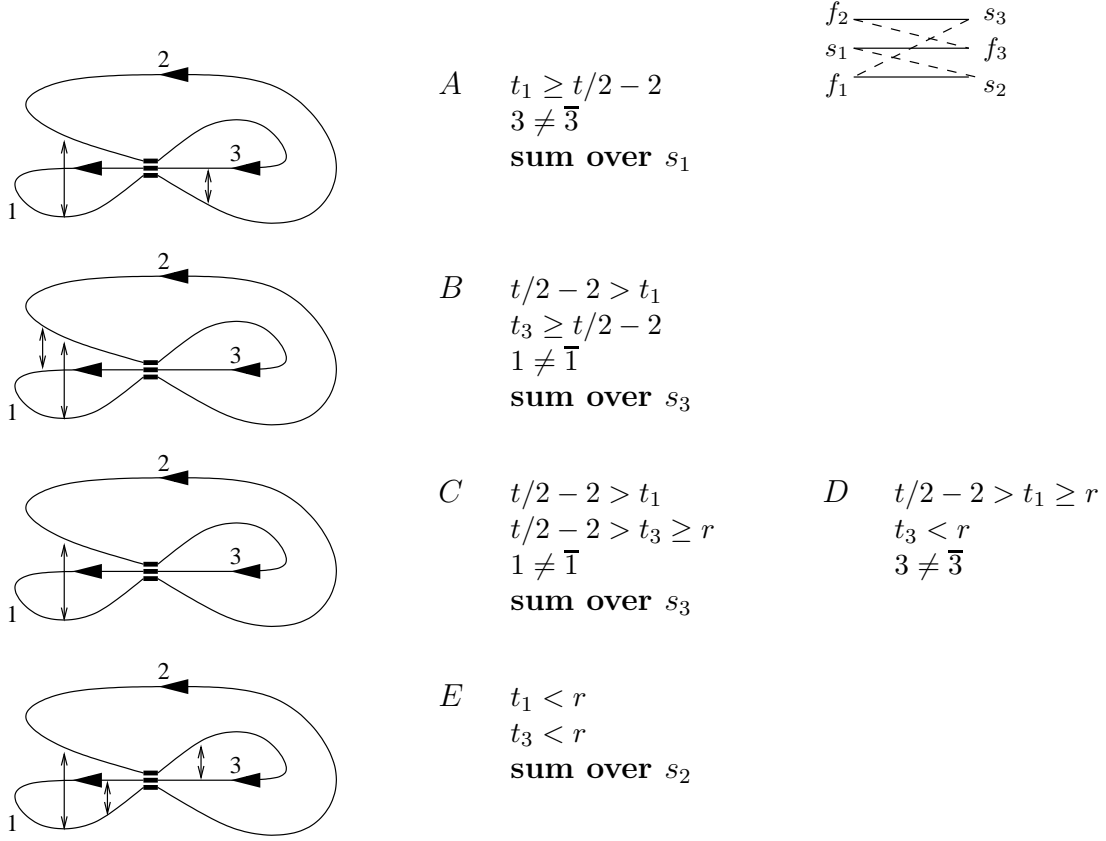


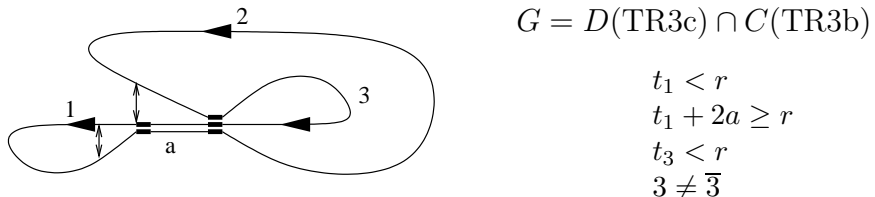
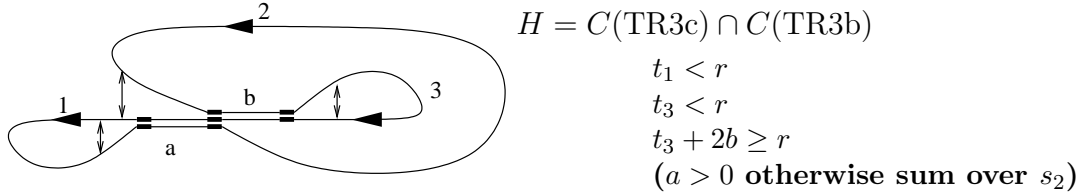
**Figure 8.** The TR3c diagram and its partition into six sets of orbits. In the upper right corner we illustrate the transitions through the intersection vertex undertaken by the original (solid lines) and the partner (dashed lines) orbits. The contribution of all sets but  $D$  can be easily shown to be zero. The set  $D$  is re-partitioned separately in Fig. 10.

The relation between TR3c and TR3b is simpler: if the lengths of an orbit from TR3c satisfy  $t_1 < r$  and  $t_3 < r$ , then we must impose restrictions  $s_1 \neq f_1$  and  $s_3 \neq f_3$ , which is reflected in the set  $F$  of Fig. 8.

Bringing the above information together we fix the partition of the diagram TR3c, Fig. 8. All five partition sets are disjoint and the contributions of the sets  $A$ ,  $B$ ,  $C$  and  $E$  evaluate to zero by summing with respect to  $s_1$ ,  $s_3$  and  $s_3$  and  $s_2$  correspondingly. The set  $A$  is slightly special since when  $t_3 \geq t/2 - 2$ , there is an additional restriction  $s_1 \neq f_2$ , but in this case one can sum over  $s_3$  to obtain the zero result.

Despite the length restriction on the sets  $C$  and  $D$ , there are still orbits belonging to these sets and the set  $C$  of TR3b. These orbits are sketched on Fig. 9. When considering the intersection of  $C$  and TR3b, we assume  $a > 0$  since when  $a = 0$ , we can sum over  $s_2$  to get zero. The contributions of this set will be evaluated separately.

The intersection of  $D$  and TR3b can be repartitioned as  $G_1$  plus  $G_2$  minus  $G_3$  with the set  $G_1$  giving zero contribution (sum over  $f_2$ ). We will show that the contributions of the sets  $G_2$  and  $G_3$  cancel each other exactly.



Decompose into the following sets

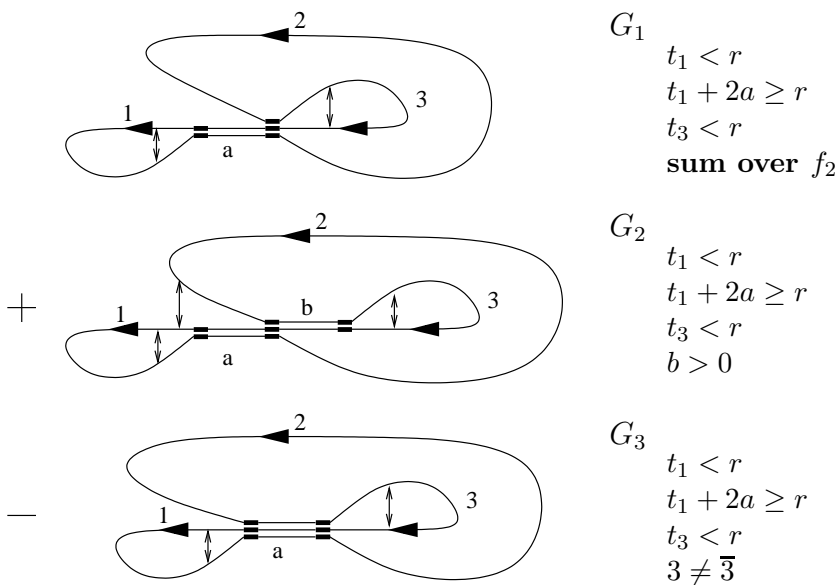


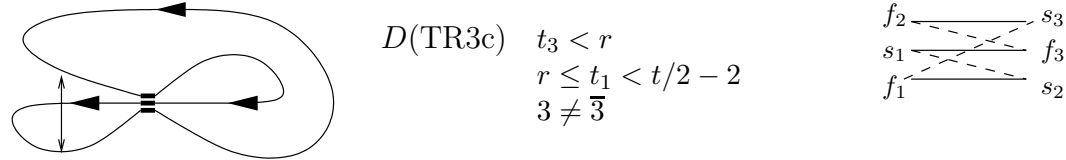
**Figure 9.** The set of orbits belonging to both set  $D$  of TR3c and set  $C$  of TR3b is repartitioned as the set  $G_1$  plus  $G_2$  minus  $G_3$ . The contribution of the set  $G_1$  is zero.

The last set to be decomposed is the set  $D$  of TR3c, see Fig. 10. Two dashed restrictions are denoting the situation when  $s_3 = f_3$  and  $s_2 = f_3$  cannot be satisfied *simultaneously*. Out of five partition sets, the sets  $D_1$  and  $D_5$  are immediately evaluated to zero, the contributions of the sets  $D_2$  and  $D_3$  clearly cancel each other, thus only the contribution of the set  $D_4$  survives.

#### 4.5. Evaluating significant diagrams

If we denote the contribution of a set  $A$  by  $|A|$ , the total contribution to the  $\tau^3$  term of the form factor expansion takes the form

$$2(K_{\text{TR3a}}(\tau) + K_{\text{TR3b}}(\tau) + K_{\text{TR3c}}(\tau)) \quad (24)$$



**Decompose into the following sets**

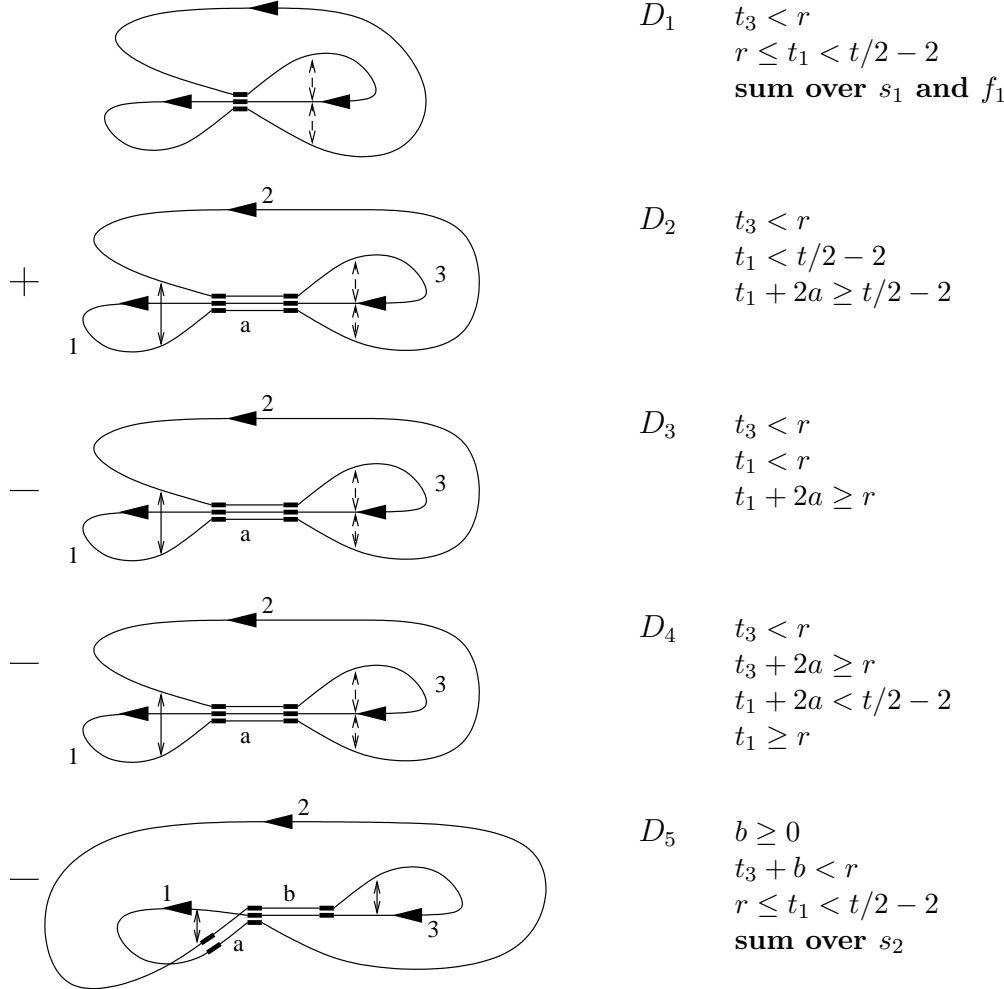


**Figure 10.** Re-partitioned set  $D$  of the TR3c diagram. Two dashed restrictions are denoting the situation when  $s_3 = f_3$  and  $s_2 = f_3$  cannot be satisfied *simultaneously*. The sets  $D_1$  and  $D_5$  give zero contribution and the sets  $D_2$  and  $D_3$  produce contributions that cancel each other.

$$= \frac{t^2}{B} (|F_2| + |F_4| + |F_5| - |E_2| + |E_3| - 2|H| - 2|D_4| - 2|G_2| + 2|G_3|).$$

The sign of each contribution is the sign displayed next to in on the corresponding diagram inverted if this diagram is from a 2-way intersection of some sets (this is true for all set but  $D_4$ ). The overall factor of two is due to the time-reversal symmetry and, in case of the sets  $F$  and  $E$ , it is cancelled by the diagram symmetry factor of 1/2, see Fig. 3.

When evaluating the contributions we use the following rules of thumb: (1) the

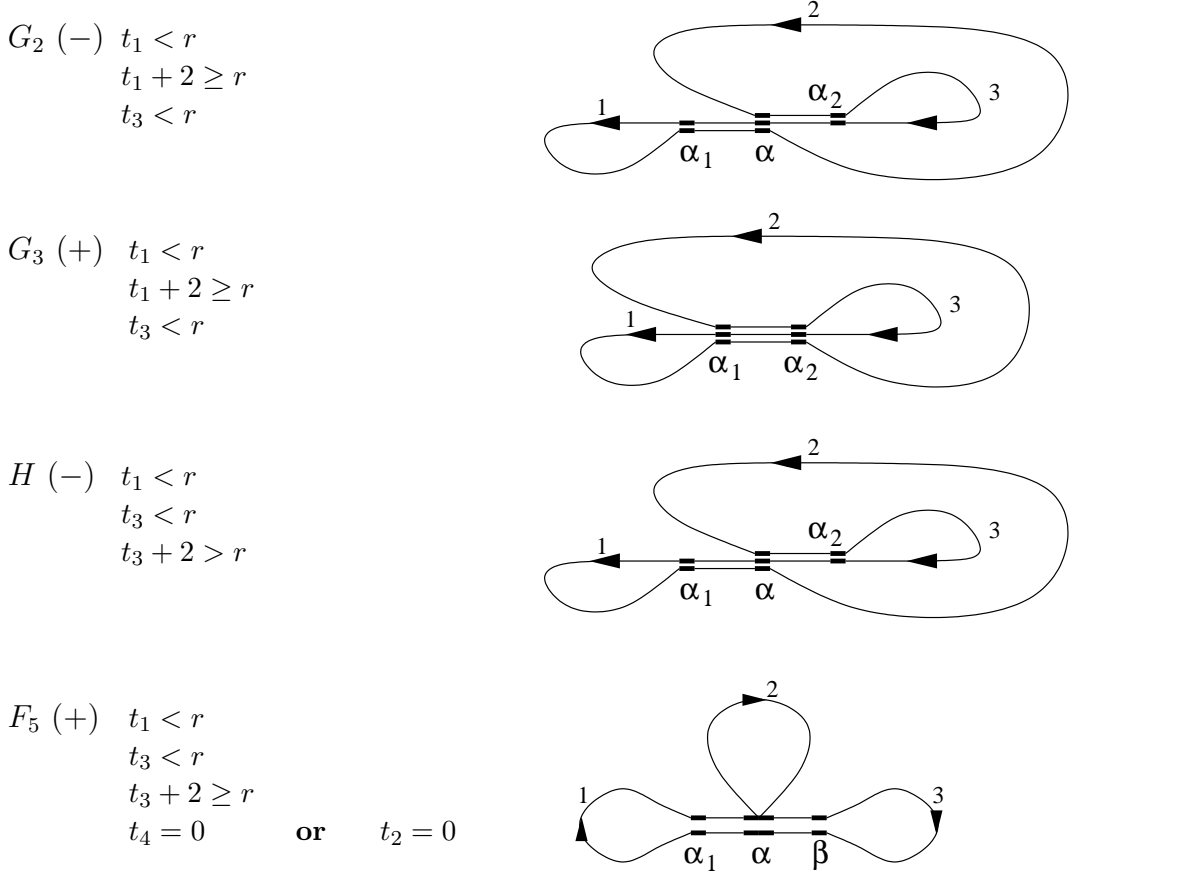


**Figure 11.** First three of the sets giving non-zero contributions

length of the tangential intersections, denoted in the diagrams by letters  $a$  and/or  $b$ , can be set to 1; (2) the restrictions can be ignored (see Appendix A for a discussion of such approximations). We also notice that all orbits belonging to the above diagrams give positive contribution (i.e. no more unitary factors left), which shows we are on the right track.

We begin by showing that the contributions of the sets  $G_2$  and  $G_3$  cancel each other. On Fig. 11 we introduced some extra notation necessary for the calculation. The contribution of the set  $G_2$  can be written as

$$|G_2| = 2 \sum_{t_3 < r} \sum_{\alpha_i} P_{(\alpha, \alpha_1) \rightarrow (\alpha_1, \alpha)}^{t_1+1} P_{(\alpha_1, \alpha) \rightarrow (\alpha, \alpha_2)}^{t_2+1} P_{(\alpha, \alpha_2) \rightarrow (\alpha_2, \alpha)}^{t_3+1} P_{(\alpha_2, \alpha) \rightarrow (\alpha, \alpha_1)}^1, \quad (25)$$

where the summation is taken over  $\alpha$ s such that there exist bonds  $(\alpha, \alpha_1)$  and  $(\alpha, \alpha_2)$  and over the ranges of  $t_i$ s outlined on the diagram. The two possible choices of  $t_1$  are expressed as the factor of 2 and thus, due to the sum  $t_1 + t_2 + t_3 + 4$  being fixed, the sum is essentially over  $t_3 < r$ . The arcs 1 and 2 are (relatively) long, therefore the corresponding transition probabilities can be approximated by their ergodic limit of  $1/B$ . We further sum over  $\alpha_1$  to obtain

$$|G_2| = \frac{2}{B^2} \sum_{t_3 < r} \sum_{\alpha_i} P_{(\alpha, \alpha_2) \rightarrow (\alpha_2, \alpha)}^{t_3+1} P_{(\alpha_2, \alpha) \rightarrow (\alpha, \alpha_1)}^1 = \frac{2}{B^2} \sum_{t_3 < r} \sum_{\alpha, \alpha_2} P_{(\alpha, \alpha_2) \rightarrow (\alpha_2, \alpha)}^{t_3+1} \quad (26)$$

We evaluate the contribution of  $G_3$  in a similar way,

$$\begin{aligned} |G_3| &= 2 \sum_{t_3 < r} \sum_{\alpha_1, \alpha_2} P_{(\alpha_2, \alpha_1) \rightarrow (\alpha_1, \alpha_2)}^{t_1+1} P_{(\alpha_1, \alpha_2) \rightarrow (\alpha_1, \alpha_2)}^{t_2+1} P_{(\alpha_1, \alpha_2) \rightarrow (\alpha_2, \alpha_1)}^{t_3+1} \\ &= \frac{2}{B^2} \sum_{t_3 < r} \sum_{\alpha_1, \alpha_2} P_{(\alpha_1, \alpha_2) \rightarrow (\alpha_2, \alpha_1)}^{t_3+1} \end{aligned} \quad (27)$$

and notice that the final expressions for  $|G_2|$  and  $|G_3|$  are identical and thus cancel each other.

The sets  $H$  and  $F_5$ , Fig. 11, on the other hand, are identical themselves. The factor of 2 before the contribution of  $H$  is compensated by the factor of 2 in the diagram  $F_5$  itself. Thus the total contribution  $|F_5| - 2|H| = 0$ .

The contributions of the sets  $E_2$ ,  $E_3$  and  $F_2$  are best grouped together. We start with  $E_3$  (evaluating only one of the two cases and multiplying it by 2), Fig. 12. To simplify the notation when dealing with numbers of order  $t$ , such as  $t/2$  and  $r$ , we ignore the constant corrections as they do not influence the limiting behaviour. The constraints imply  $t_1 = r - 2$  and  $t_1 + t_2 = t/2 \pm \text{const}$ , therefore the summation is over  $t_3$  (or  $t_4$ ). The summation is limited by the constraint  $t_3 > r$  on one side and by  $t_3 < t - t_1 - t_2 \approx t/2$  on the other.

$$\begin{aligned} |E_3| &= 4 \sum_{r < t_3 < \frac{t}{2}} \sum_{\alpha, \alpha_1, \beta, \beta_1} P_{(\beta, \beta_1) \rightarrow (\alpha_1, \alpha)}^{t_1+1} P_{(\alpha_1, \alpha) \rightarrow (\beta_1, \beta)}^{t_2+1} P_{(\beta_1, \beta) \rightarrow (\alpha_1, \alpha)}^{t_3+1} P_{(\alpha_1, \alpha) \rightarrow (\beta, \beta_1)}^{t_4+1} \\ &= \frac{4}{B^3} \sum_{r < t_3 < \frac{t}{2}} \sum_{\alpha, \alpha_1, \beta, \beta_1} P_{(\alpha_1, \alpha) \rightarrow (\beta, \beta_1)}^{t_4+1} = \frac{4}{B^3} \sum_{r < t_3 < \frac{t}{2}} \sum_{\alpha, \alpha_1} 1 = \frac{4}{B^2} \left( \frac{t}{2} - r \right), \end{aligned} \quad (28)$$

where to perform the summation over all possible bonds  $(\beta, \beta_1)$  we invoke the probability conservation and the summation over all possible bonds  $(\alpha, \alpha_1)$  is just the number of the bonds.

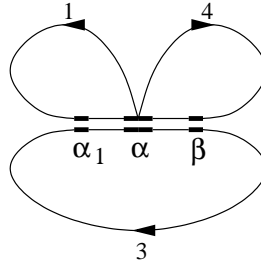
For  $E_2$  the situation is very similar, but we choose to sum over  $t_4$ ,

$$\begin{aligned} |E_2| &= 4 \sum_{t_4 < \frac{t}{2} - r} \sum_{\alpha, \alpha_1, \beta} P_{(\beta, \alpha) \rightarrow (\alpha_1, \alpha)}^{t_1+1} P_{(\alpha, \beta) \rightarrow (\alpha_1, \alpha)}^{t_2+1} P_{(\alpha_1, \alpha) \rightarrow (\beta, \alpha)}^{t_3+1} P_{(\alpha_1, \alpha) \rightarrow (\alpha, \beta)}^1 \\ &= \frac{4}{B^2} \sum_{t_4 < \frac{t}{2} - r} \sum_{\alpha, \alpha_1, \beta} P_{(\alpha_1, \alpha) \rightarrow (\beta, \alpha)}^{t_4+1} P_{(\alpha_1, \alpha) \rightarrow (\alpha, \beta)}^1 \\ &= \frac{4}{B^2} \sum_{t_4 < \frac{t}{2} - r} \sum_{\alpha, \alpha_1} P_{(\alpha_1, \alpha) \rightarrow (\alpha, \alpha_1)}^{t_4+2}, \end{aligned} \quad (29)$$

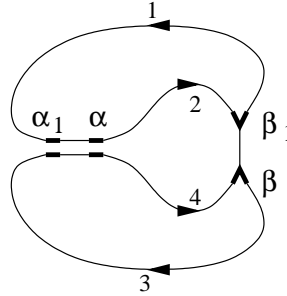
where, to get to the last line, we used the symmetry of the time-reversal invariance,  $P_{(\alpha_1, \alpha) \rightarrow (\alpha, \beta)} = P_{(\beta, \alpha) \rightarrow (\alpha, \alpha_1)}$ , and the Markov property of the probabilities. Unfortunately, the contribution of  $E_2$  depends on particular structure of short orbits of the graph. Hopefully, the other contributions will help:

$$\begin{aligned} |F_2| &= 4 \sum_{t_3 < r} \sum_{\alpha, \alpha_1, \beta} P_{(\alpha, \alpha_1) \rightarrow (\alpha_1, \alpha)}^{t_1+1} P_{(\alpha_1, \alpha) \rightarrow (\alpha, \beta)}^{t_2+1} P_{(\alpha, \beta) \rightarrow (\beta, \alpha)}^{t_3+1} P_{(\beta, \alpha) \rightarrow (\alpha, \alpha_1)}^1 \\ &= \frac{4}{B^2} \sum_{t_3 < r} \sum_{\alpha, \alpha_1, \beta} P_{(\alpha, \beta) \rightarrow (\beta, \alpha)}^{t_3+1} P_{(\beta, \alpha) \rightarrow (\alpha, \alpha_1)}^1 = \frac{4}{B^2} \sum_{t_3 < r} \sum_{\alpha, \beta} P_{(\alpha, \beta) \rightarrow (\beta, \alpha)}^{t_3+1}, \end{aligned} \quad (30)$$

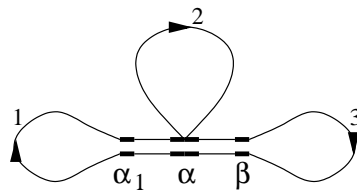
$$E_2 (-) \quad \begin{aligned} t_1 + t_2 + 2 &\geq t/2 \\ t_1 + t_2 &< t/2 \\ t_2 = 0 & \quad \text{or} \quad t_4 = 0 \\ t_3 + 1 \geq r & \quad t_1 + 1 \geq r \end{aligned}$$



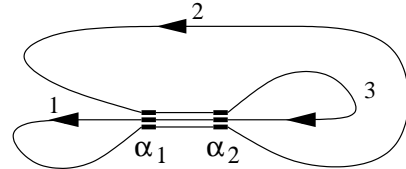
$$E_3 (+) \quad \begin{aligned} t_1 + t_2 + 2 &\geq t/2 \\ t_1 + t_2 &< t/2 \\ t_1 + 1 < r & \quad t_3 + 1 < r \\ t_1 + 2 \geq r & \quad \text{or} \quad t_3 + 2 \geq r \\ t_3 + 1 \geq r & \quad t_1 + 1 \geq r \end{aligned}$$



$$F_2 (+) \quad \begin{aligned} t_1 + 2 &\geq r \\ t_1 &< r \\ t_3 &< r \\ t_4 = 0 & \quad \text{or} \quad t_2 = 0 \end{aligned}$$



$$D_4 (-) \quad \begin{aligned} t_3 &< r \\ t_3 + 2 &\geq r \\ t_1 &\geq r \\ t_1 + 2 &< t/2 - 2 \end{aligned}$$



$$F_4 (+) \quad \begin{aligned} t_1 + 2 &\geq r \\ t_1 &< r \\ t_3 + 2 &\geq r \\ t_3 &< r \end{aligned}$$

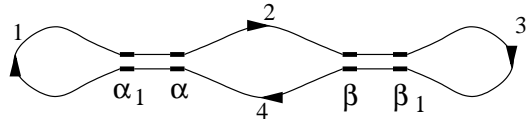


**Figure 12.** Sets  $E_2$ ,  $E_3$ ,  $F_2$ ,  $D_4$  and  $F_4$  giving non-zero contributions. The diagram of  $E_2$  was “symmetrized” to highlight its similarity with  $F_2$

where to get the final result we summed over  $\alpha_1$  and invoked the probability conservation. We notice that the sums in (30) and (29) are identical, up to a variable change, apart from the upper limit of the sum. Assuming, without loss of generality, that  $r > \frac{t}{2} - r$ , we obtain

$$|F_2| - |E_2| = \frac{4}{B^2} \sum_{\frac{t}{2} - r \leq t_3 < r} \sum_{\alpha, \beta} P_{(\alpha, \beta) \rightarrow (\beta, \alpha)}^{t_3+1}, \quad (31)$$

but now the sum is over large values of  $t_3$ , thus

$$|F_2| - |E_2| = \frac{4}{B^3} \sum_{\frac{t}{2}-r \leq t_3 < r} \sum_{\alpha, \beta} 1 = \frac{4}{B^2} \left( r - \left( \frac{t}{2} - r \right) \right). \quad (32)$$

Bringing it together with  $|E_3|$ , we obtain

$$|F_2| - |E_2| + |E_3| = \frac{4r}{B^2} \quad (33)$$

The next set to evaluate is  $D_4$ , Fig. 12. All arcs are long in this case, leading to the contribution

$$\begin{aligned} |D_4| &= 2 \sum_{r \leq t_1 < \frac{t}{2}} \sum_{\alpha_1, \alpha_2} P_{(\alpha_2, \alpha_1) \rightarrow (\alpha_1, \alpha_2)}^{t_1+1} P_{(\alpha_1, \alpha_2) \rightarrow (\alpha_1, \alpha_2)}^{t_2+1} P_{(\alpha_1, \alpha_2) \rightarrow (\alpha_2, \alpha_1)}^{t_3+1} \\ &= \frac{2}{B^3} \sum_{r \leq t_1 < \frac{t}{2}} \sum_{\alpha_1, \alpha_2} 1 = \frac{2}{B^2} \left( \frac{t}{2} - r \right). \end{aligned} \quad (34)$$

In the final contribution, coming from the set  $F_4$  of Fig. 12, the summation is over  $t_2 + t_4 \approx t - 2r$ . The arcs 1 and 3 are both long and of fixed length  $r - 1$  or  $r - 2$ . This freedom of choice gives rise to the 4 factor in front of the sum,

$$|F_4| = \frac{4}{B^2} \sum_{t_2+t_4=t-2r} \sum_{\alpha, \alpha_1, \beta, \beta_1} P_{(\alpha_1, \alpha) \rightarrow (\beta, \beta_1)}^{t_2+1} P_{(\beta_1, \beta) \rightarrow (\alpha, \alpha_1)}^{t_4+1}, \quad (35)$$

where the terms corresponding to the arcs 1 and 3, have already being approximated by  $1/B$ . At least one of the arcs, 2 or 4 is long. Assuming, without loss of generality, that 2 is long, we have for the inner sum,

$$\sum_{\alpha, \alpha_1, \beta, \beta_1} P_{(\alpha_1, \alpha) \rightarrow (\beta, \beta_1)}^{t_2+1} P_{(\beta_1, \beta) \rightarrow (\alpha, \alpha_1)}^{t_4+1} = \frac{1}{B} \sum_{\alpha, \alpha_1, \beta, \beta_1} P_{(\beta_1, \beta) \rightarrow (\alpha, \alpha_1)}^{t_4+1} = \frac{1}{B} \sum_{\beta, \beta_1} 1 = 1. \quad (36)$$

Thus the result for the set  $F_4$  is

$$|F_4| = \frac{4}{B^2} \sum_{t_2+t_4=t-2r} 1 = \frac{4(t-r-r)}{B^2} \quad (37)$$

The overall result is therefore

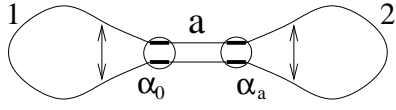
$$\begin{aligned} 2(K_{\text{TR3a}}(\tau) + K_{\text{TR3b}}(\tau) + K_{\text{TR3c}}(\tau)) &= \frac{t^2}{B} (|F_4| + |F_2| - |E_2| + |E_3| - 2|D_4|) \\ &= \frac{t^2}{B} \left( \frac{4}{B^2} (t-r-r) + \frac{4}{B^2} r - \frac{4}{B^2} \left( \frac{t}{2} - r \right) \right) = \frac{2t^3}{B^3} \rightarrow 2\tau^3. \end{aligned} \quad (38)$$

Taking into account that  $K_{\text{NTR3a}}(\tau) + K_{\text{NTR3b}}(\tau) = 0$  [10], we obtain the final result  $K_{\text{TR3}}(\tau) = 2\tau^3$ , QED.

## 5. Conclusions

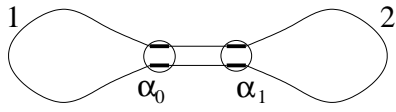
The results of this manuscript complement those of [10] to form the derivation of the form factor of *generic* quantum graphs to the third order.

While the derivation presented above is quite technical, the underlying idea is beautiful in its simplicity: the set of all orbits can be partitioned in such a way that the



$$t_1 < t/2$$

$$t_1 + 2a \geq t/2$$



$$a = 1$$

$$t_1 < t/2$$

$$t_1 + 2 \geq t/2$$

**Figure A1.** In the first set, the tangential intersection must be of length  $a > 0$ . In the second set, the length of the intersection is not explicitly specified. It turns out that both sets contain exactly the same orbits.

contribution of each partition set can be easily shown to be zero. And this can be done without evaluating the contributions of individual orbits! The nonzero “correct” result then arises from the intersections of the partition sets. The orbits in such intersections have generic properties: most of their arcs are long, making direct evaluation possible.

We presented one of the possible partitions and obtained the expected RMT result. The partition is based upon three basic diagrams, each being separately partitioned. It is very possible that there exists a “unified” diagram with a simple partition. If such diagram is found, it might make possible the derivation to all orders. Alas, it has so far evaded all attempts to find it.

## 6. Acknowledgments

The idea of the evaluation of the TR2 diagram, as it is done in Section 4.1, was born in the discussion with Holger Schanz during the author’s visit to Max-Planck-Institut, Göttingen, Germany. This idea later become the foundation for this entire work. The author is extremely grateful to Robert Whitney who proofread the manuscript, pointed out numerous mistakes and proposed simplifications. A part of the research was performed while the author was working at the Weizmann Institute of Science, Rehovot, Israel, supported by the Israel Science Foundation, a Minerva grant, and the Minerva Center for Nonlinear Physics. This, and the encouragement provided by U. Smilansky, is greatly appreciated.

## Appendix A. Setting $a = 1$ in TR2 diagram

When we evaluated the contribution of the TR2 orbits, we dropped the constraints and set the length of tangential intersection  $a$  to 1 (Fig. A1). Here we discuss various aspects of this approximation.

First of all, in the case of TR2, it is not an approximation at all. However it is not clear whether the proof of such claim can be extended to more complicated sets of orbits. We therefore provide a condition which is easier to generalise and which is not

too restrictive.

Consider the case  $a = 2$ . In this case the orbit self-intersect along three vertices,  $\alpha_0, \alpha_1, \alpha_2$ . Summing over all possible¶ arcs 1 and 2 we get

$$\frac{t^2}{2B} \sum_{\alpha_0, \alpha_1, \alpha_2} P_{(\alpha_1, \alpha_0) \rightarrow (\alpha_0, \alpha_1)}^{t_1+1} P_{(\alpha_1, \alpha_2) \rightarrow (\alpha_2, \alpha_1)}^{t_2+1} \sigma_{\alpha_0 \alpha_2}^{\alpha_1} \sigma_{\alpha_2 \alpha_0}^{\alpha_1} \sigma_{\alpha_0 \alpha_2}^{\alpha_1*} \sigma_{\alpha_2 \alpha_0}^{\alpha_1*}. \quad (\text{A.1})$$

Both  $t_1$  and  $t_2$  are now long (they are restricted by the inequalities  $t_1 = t - t_2 < t/2$  and  $t_1 + 2a \geq t/2$ ), so the final expression is

$$\frac{t^2}{2B^3} \sum_{\alpha_0, \alpha_1, \alpha_2} |\sigma_{\alpha_0 \alpha_2}^{\alpha_1}|^4. \quad (\text{A.2})$$

Under very reasonable conditions on the transfer matrix we would have  $\sum |\sigma_{\alpha_0 \alpha_2}^{\alpha_1}|^4 = o(B)$ , therefore the expression (A.2) tends to zero as  $t, B \rightarrow \infty$ . When calculating the contribution of the orbits with  $a = 1$ , we can ignore the restrictions  $s_1 \neq f_1$  and  $s_2 \neq f_2$ : they only serve to disallow counting orbits with  $a > 1$ , but we have shown that these do not change the limiting behaviour.

## References

- [1] Bohigas O, Giannoni M J and Schmit C 1984 *Phys. Rev. Lett.* **52** 1–4
- [2] Haake F 2000 *Quantum Signatures of Chaos* (Springer, Berlin)
- [3] Berry M V 1985 *Proc. R. Soc. Lond. A* **400** 229–51
- [4] Sieber M and Richter K 2001 *Physica Scripta* bf T90 128
- [5] Sieber M 2002 *J. Phys. A* **35** L613–L619  
(Sieber M 2002 *Preprint* nlin.CD/0209016)
- [6] Gutzwiller M C 1971 *J. Math. Phys.* **12** 343–58
- [7] Kottos T and Smilansky U 1997 *Phys. Rev. Lett.* **79** 4794–7
- [8] Kottos T and Smilansky U 1999 *Ann. Phys.* **274** 76–124
- [9] Berkolaiko G, Schanz H and Whitney R S 2002 *Phys. Rev. Lett.* **88** 104101
- [10] Berkolaiko G, Schanz H and Whitney R S 2002 *Preprint* nlin.CD/0205014
- [11] Mehta M L 1991 *Random Matrices* (Academic Press, New York)
- [12] Barra F and Gaspard P 2000 *J. Stat. Phys.* **101** 283–319
- [13] Grimmett G R and Stirzaker D R 1992 *Probability and Random Processes* (Clarendon Press, Oxford)
- [14] Tanner G 2001 *J. Phys. A* **34** 8485

¶ We are ignoring the constraints here, thus overcounting some orbits with  $a > 2$ . But the contribution of such orbits is going to be even smaller than for  $a = 2$